remote sensing

MDPI

Article

Pseudorange Bias Analysis and Preliminary Service Performance Evaluation of BDSBAS

Yuchen Liu [1,2], Yueling Cao [1,*], Chengpan Tang [1], Jinping Chen [3], Liqian Zhao [4], Shanshi Zhou [1], Xiaogong Hu [1], Qiuning Tian [1,2] and Yufei Yang [3]

[1] Shanghai Astronomical Observatory, Chinese Academy of Sciences, Shanghai 200030, China; liuyuchen@shao.ac.cn (Y.L.); cptang@shao.ac.cn (C.T.); sszhou@shao.ac.cn (S.Z.); hxg@shao.ac.cn (X.H.); tianqiuning@shao.ac.cn (Q.T.)
[2] University of Chinese Academy of Sciences, Beijing 100049, China
[3] Beijing Navigation Center, Beijing 100094, China; jinping_chen@sina.com (J.C.); gnssyyf@163.com (Y.Y.)
[4] Space Star Technology Co., Ltd., Beijing 100095, China; zhaoliqian@shao.ac.cn
* Correspondence: caoyueling@shao.ac.cn

Abstract: To satisfy the demands of civil aviation organizations and other users of satellite navigation systems for high-precision and high-integrity service performance, many countries and regions have established satellite-based augmentation systems (SBAS) referring to the Radio Technical Commission for Aeronautics (RTCA) service standards and agreements. The BeiDou SBAS (BDSBAS) provides both single-frequency service, which augments Global Positioning System (GPS) L1 C/A signal, and dual-frequency multi-constellation (DFMC) service, which augments BeiDou Navigation Satellite System (BDS) B1C and B2a dual frequency signals presently, meeting the requirements of the RTCA DO-229D protocol and the SBAS L5 DFMC protocol requirements, respectively. As one of the main error sources, the pseudorange bias errors of BDSBAS monitoring receivers were estimated and their effect on the performance of the BDSBAS service was analyzed. Based on the user algorithms of SBAS differential corrections and integrity information, the service accuracy, integrity, and availability of the BDSBAS were evaluated using real observation data. The results show that the maximum of monitoring receiver pseudorange bias errors between L1P and L1P/L2P can reach 1.57 m, which become the most important errors affecting the performance of the BDSBAS service. In addition, the results show that the pseudorange bias of GPS BlockIII is the smallest, while that of GPS BlockIIR is the largest. Compared with the positioning accuracy of the open service of the core constellation, the positioning accuracy of the BDSBAS service can be improved by approximately 47% and 36% for the RTCA service and DFMC service, respectively. For RTCA services, the protection limit (PL) calculated with the integrity information can 100% envelop the positioning error (PE) and no integrity risk event is detected. The service availability of BDSBAS for APV-I approach is approximately 98.8%, which is mainly affected by the availability of ionospheric grid corrections in the service marginal area. For DFMC service, the integrity risk is not detected either. The service availability for CAT-I approach is 100%. Improving the availability of ionospheric grid corrections is one of the important factors to improve service performance of BDSBAS RTCA service.

Keywords: BDSBAS; pseudorange bias; accuracy; integrity; availability

Citation: Liu, Y.; Cao, Y.; Tang, C.; Chen, J.; Zhao, L.; Zhou, S.; Hu, X.; Tian, Q.; Yang, Y. Pseudorange Bias Analysis and Preliminary Service Performance Evaluation of BDSBAS. *Remote Sens.* **2021**, *13*, 4815. https://doi.org/10.3390/rs13234815

Academic Editors: Kamil Krasuski and Prasad S. Thenkabail

Received: 2 September 2021
Accepted: 25 November 2021
Published: 27 November 2021

1. Introduction

With the continuous development and construction of satellite navigation systems, there are currently four global navigation satellite systems (GNSS), namely: the Global Positioning System (GPS), Global Navigation Satellite System (GLONASS), Galileo and BeiDou Navigation Satellite System (BDS), and regional navigation satellite systems, such as Quasi-Zenith Satellite System (QZSS) and Indian Regional Navigation Satellite System (IRNSS) [1]. Satellite navigation systems are widely used in positioning, navigation, and

timing (PNT) services and can satisfy the basic requirements of various users [2,3]. However, when the GNSS continues to expand its application areas, high-end users, such as those in precision agriculture, ports, and civil aviation, have introduced higher standards of use requirements for its positioning accuracy, integrity, and availability [4]. In this case, some countries and regions have established satellite-based augmentation systems (SBAS) to compensate for the lack of service performance in satellite navigation and positioning, including the European Geostationary Navigation Overlay Service (EGNOS), the United States' Wide Area Augmentation System (WAAS), Russia's System for Differential Correction and Monitoring (SDCM), Japan's Multifunctional Satellite Augmentation System (MSAS), India's GPS = Aided Geo Augmented Navigation (GAGAN), and China's BeiDou SBAS (BDSBAS) [4–7].

Currently, the BDSBAS provides GPS L1C/A single-frequency enhancement services under the Radio Technical Commission for Aeronautics (RTCA) agreement and BDS-3 B1C/B2a dual-frequency enhancement services under the dual-frequency multi-constellation (DFMC) agreement [5–7]. In contrast, other SBASs currently only provide RTCA single-frequency services. SBAS broadcasts clock–ephemeris corrections, ionospheric grid delay corrections, and corresponding integrity monitoring information to users through GEO satellites, and users improve the accuracy of positioning by receiving SBAS messages. However, the residual errors, which are not provided to users, will affect the service accuracy and integrity performance of SBAS users [7,8]. Especially for dual-frequency users, the dual-frequency combination will amplify the magnitude of uncorrected errors. If there is an error that is not deducted on the service layer, the error will be amplified and passed to the user.

The main sources of errors that affect satellite navigation services include clock–ephemeris prediction errors, tropospheric delay errors, ionospheric delay errors, pseudorange biases, and errors of pseudorange multipath and noise errors [8–10]. Zhao et al. [11] evaluated the accuracy of the BDS-3 satellite broadcast ephemeris, and the results showed that the space signal accuracy of the BDS-3 broadcast ephemeris was approximately 0.5 m [11]. The zenith tropospheric delay (ZTD) was approximately 2.3 m. When the satellite altitude angle is low, the slant path delay can reach 20 m [12]; SBAS broadcasts grid corrections to users. Generally, the correction accuracy of the ionospheric grid model is better than 0.5 m [13]. Multipath and noise can have the largest impact on the ranging accuracy on the order of meters [14,15]. The pseudorange bias has not received much attention, but its impact can also reach the order of meters [16,17].

Pseudorange bias is the constant bias of pseudorange measurement caused by the non-ideal characteristics of satellite navigation signals [17,18]. Pseudorange bias was first discovered in 1993. The downlink signal of GPS Block II satellite SVN19 was abnormal, and the pseudorange measurement of different types of receivers appeared with different deviations, which caused a significant decrease in the accuracy of user differential positioning [19].

For the main process of BDSBAS, the main control station collects real-time monitoring station data, which mainly include the pseudorange and carrier phase observations, performs the calculation of differential integrity information within the validity period of the data, and broadcasts it to users through GEO satellites [20]. The pseudorange residual, including the receiver clock error, is one of the important inputs to calculate the corrections and integrity information. When calculating the clock corrections, the receiver clock error of the master control station is fixed, and the least square method is used to calculate the clock corrections and receiver clock error of each monitoring station in real time [8,21]. Since the receiver clock error cannot absorb the errors from the satellite and atmosphere (mainly includes ionospheric delay and tropospheric delay), if the errors cannot be correctly suppressed and weakened, the correctness of the clock correction will be affected. Simultaneously, the residual errors of the uncorrected errors will be passed to the user through the integrity information, which will affect the service performance of the system.

At present, the error sources that affect the BDSBAS mainly include clock–ephemeris errors, ionospheric delay, tropospheric delay, multipath noise, and the pseudorange bias, and there are already some effective correction methods to eliminate these observation errors. However, pseudorange bias is a kind of error that has not been widely recognized. It shows that the pseudorange bias is an error related to the receiver's frontend filter bandwidth, correlator spacing, and anti-multipath algorithm [16–18,21]. Unlike other sources of error in the pseudorange, receivers of different technical states have differences in the pseudorange of the same satellite, and the biases of different frequencies are not the same either. So, we call it the pseudorange bias. Therefore, even if the status of SBAS's receiver and the status of users' receiver are the same, if the frequency used by the user and the SBAS are inconsistent, there will still be a pseudorange bias. In most cases, the receiver status of the user and the SBAS are not consistent, so the influence of the pseudorange bias is more serious. The definition and extraction method of the pseudorange bias and its effect on the performance of satellite-based augmentation services are analyzed in detail below [22–24].

Various errors can affect the performance of SBAS services. Among them, the correction methods for some error sources are relatively mature, such as the tropospheric delay correction and multipath and noise smoothing, but pseudorange bias correction has not been widely recognized. Although most of the error sources are as same as the Radio Navigation Satellite System (RNSS) [25], the indicator of the BDSBAS (H: 1 m/1.5 m V: 1.5 m/2 m) is more demanding then RNSS (3D:10 m). Therefore, we need to clarify the impact of these errors on the service.

Studies have shown that both WAAS and EGNOS can provide positioning performance [9,26–28] at a level better than 1.5 m in the horizontal direction and better than 2 m in the vertical direction in the service area [29]. Users can calculate the protection limit (PL) through the integrity parameter [30], which represents the reliability of the location information calculated by the user, based on the differential corrections. The PL includes the horizontal PL (HPL) and vertical PL (VPL), and the envelope ability of the PL to the positioning error (PE) can reflect the integrity performance of SBAS services. In addition, to satisfy the Approach with Vertical Guidance-1 (APV-1) and Category-1 (CAT-1) services, the availability of SBAS services can be further analyzed through the PL. In this paper, the analysis method of the service performance of the BDSBAS is studied. The service accuracy, integrity, and availability of the BDSBAS are initially analyzed using the BDSBAS-measured data [31–33].

With this background, firstly, based on the measured data from the BDSBAS monitoring stations, we extract the pseudorange bias between receivers of different manufacturers through the collocated receiver method, to confirm the existence and magnitude of the pseudorange bias. Then we use multi-station, multi-satellite, and multi-day data to calculate the GPS pseudorange bias between L1P and L1P/L2P based on the least square method, and conduct short-term and long-term monitoring. Then, the extracted pseudorange bias is corrected to the clock corrections, and is broadcast to the users. Finally, we receive the SBAS product broadcast by GEO satellites through the user receiver, and we evaluate and analyze the user's positioning performance, availability, continuity, and integrity. Section 2 introduces the collocated receiver method, the main methods of calculating the GPS pseudorange bias, and the method to evaluate the performance of BDSBAS. The data and the processing strategies of calculating pseudorange bias and performance analysis are presented in Section 3. Section 4 shows the magnitude of the pseudorange bias and its influence on positioning performance, and the result of the user's positioning performance, availability, continuity, and integrity after the pseudorange bias is corrected. In the last part, we make some conclusions and discussions.

2. Methods

This section introduces the method used to extract the pseudorange bias. Then based on the above method, a method of extracting the pseudorange bias based on BDSBAS

RTCA service is proposed. Finally, the method to evaluate the performance of BDSAS is introduced.

2.1. Collocated Receiver Method

Due to the nonideal characteristics of downlink navigation signals of navigation satellites, receivers of different manufacturers (i.e., those with different technical statuses) produce constant biases of different sizes and symbols for the downlink navigation signal, which we call the pseudorange bias. For the same nonideal downlink navigation signal of the same satellite, the pseudorange bias is related to the receiver's frontend filter bandwidth, correlator spacing, and anti-multipath algorithm [16–18]. They lead to different satellites and different frequencies with different pseudorange biases. To analyze the characteristics of the pseudorange bias, pseudorange observations from collocated receivers with distances of several meters were used. The collocated receiver pseudorange observation equations are as follows [34]:

$$\begin{cases} P_{r1}^{i}(L_j) = \rho_{r1}^{i} + c*(\delta t_{r1} - \delta t^{i}) + c*(DCB_{r1}^{L_j} + DCB_{j}^{L_j}) + \dfrac{TEC^{i}}{f_j^2} + T_{r1}^{i} + rel_{r1}^{i} + \alpha_{r1}^{i}(L_j) + \varepsilon_{r1}^{i} \\ P_{r2}^{i}(L_j) = \rho_{r2}^{i} + c*(\delta t_{r2} - \delta t^{i}) + c*(DCB_{r2}^{L_j} + DCB_{j}^{L_j}) + \dfrac{TEC^{i}}{f_j^2} + T_{r2}^{i} + rel_{r2}^{i} + \alpha_{r2}^{i}(L_j) + \varepsilon_{r2}^{i} \end{cases} \quad (1)$$

where $P_{r1}^{i}(L_j)$ is the pseudorange of the collocated receivers; ρ_{r1}^{i} is the range between satellite and receiver; L_j is the frequency of the pseudorange; δt_{r1} and δt^{i} are the clock errors of the receiver and satellite; $DCB_{r1}^{L_j}$ and $DCB_{j}^{L_j}$ are the receiver and satellite differential code biases (DCB) parameters, respectively; $\frac{TEC^{i}}{f_j^2}$ and T_{r1}^{i} are the ionosphere delay and troposphere delay, respectively; rel_{r1}^{i} is the relativity error; ε_{r1}^{i} is the multipath-noise error; $\alpha_{r1}^{i}(L_j)$ is the pseudorange bias.

The range between satellite and receiver can be calculated with the broadcast ephemeris of the satellite and known coordinates of the receiver. The measurement that eliminates the range from the pseudorange is expressed as observation minus computation (OC). Since common errors such as satellite clock errors, satellite DCB parameters, satellite ephemeris errors, ionospheric delays, tropospheric delays, and relativity errors are almost identical between two collocated receivers of the same satellite, they can be eliminated with a single difference in OC measurements. The results include the difference in receiver clock errors, receiver DCB parameters, the pseudorange biases, and observation noises. The receiver clock error and receiver DCB parameter are identical for all satellites, and they can be removed with the double difference of OC measurements, according to a reference satellite, as shown in Equation (2).

$$\begin{cases} OC_{r1}^{i} = P_{r1}^{i}(L_j) - \rho_{r1}^{i} \\ OC_{r1}^{i} - OC_{r2}^{i} = c*(\delta t_{r1} - \delta t_{r2} + DCB_{r1}^{L_j} - DCB_{r2}^{L_j}) + \varepsilon_{r1}^{i} - \varepsilon_{r2}^{i} + \alpha_{r1}^{i}(L_j) - \alpha_{r2}^{i}(L_j) \\ dt\alpha_{r1-r2}^{i-k} = OC_{r1}^{i} - OC_{r2}^{i} - (OC_{r1}^{k} - OC_{r2}^{k}) \\ = \alpha_{r1}^{i}(L_j) - \alpha_{r2}^{i}(L_j) - (\alpha_{r1}^{i}(L_j) - \alpha_{r2}^{i}(L_j)) + \varepsilon_{r1}^{i} - \varepsilon_{r2}^{i} - (\varepsilon_{r1}^{k} - \varepsilon_{r2}^{k}) \end{cases} \quad (2)$$

where $OC_{r1}^{i} - OC_{r2}^{i}$ is the single difference between the collocated receiver; $dt\alpha_{r1-r2}^{i-k}$ is the double difference between the satellite i and satellite k, based on the collocated receiver; Since observation noises ε_{r1}^{i} are white noise considered with zero mean values, the mean value of $dt\alpha_{r1-r2}^{i-k}$ for a period of double difference track that commonly spans at least 24 h is subtracted out as the pseudorange bias for the L_j signal.

2.2. Calculation Method of Pseudorange Bias

The pseudorange bias will be amplified by the dual-frequency ionospheric-free combination, which will affect SBAS differential corrections and integrity information processing. BDSBAS uses the L1P and L2P dual-frequency pseudorange data of the monitoring receivers to calculate GPS clock differential corrections, and these corrections are used by

GPS L1C/A single-frequency users to correct the satellite clock errors. For the GPS single-frequency users, the DCB between GPS L1C/A and GPS L1P should be corrected, because the datum of GPS broadcast ephemeris and SBAS messages is L1P/L2P. Therefore, the pseudorange bias we discussed is between L1P and L1P/L2P. As BDS users use B1C/B2a dual-frequency pseudorange data and the SBAS corrections are also solved by B1C/B2a, the pseudorange bias is largely self-consistent. Therefore, we mainly discuss the impact of pseudorange bias on the RTCA service of BDSBAS. Due to the inconsistency between the pseudorange biases in single-frequency observation and dual-frequency ionospheric-free combination, an additional error will be involved in the SBAS RTCA service observation equation, as shown in Equation (3).

$$OC_{L1CA} = P_{L1CA} - DCB_{p1c1} - s - \varepsilon_{err} - SBAS_{corr} + \alpha_{L1P} - \alpha_{L1P/L2P} \quad (3)$$

where OC_{L1CA} is the L1 frequency pseudorange residual error; P_{L1CA} is the pseudorange observation; α_{L1P} is the pseudorange bias in L1 frequency signal; $\alpha_{L1P/L2P}$ is the pseudorange bias contained in the SBAS satellite clock differential corrections; s is the range between satellite and receiver; ε_{err} are the observation common errors; $SBAS_{corr}$ is the projection of SBAS orbital and clock differential corrections in user line of sight; DCB_{p1c1} is the DCB between L1CA and L1P.

To weaken the influence of the pseudorange bias on SBAS correction, the pseudorange bias difference ($\alpha_{L1P} - \alpha_{L1P/L2P}$) between the L1P single-frequency and L1P/L2P dual-frequency ionospheric-free combination should be estimated and corrected from the SBAS satellite clock differential correction. The calculation method is described in detail in Equations (4) and (5) and the processing is shown in Figure 1.

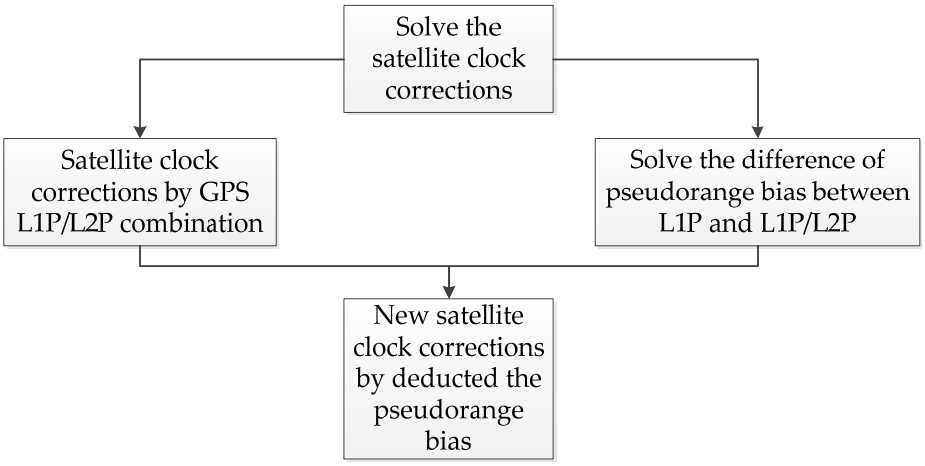

Figure 1. Process to deduce the pseudorange bias and form new satellite clock corrections.

Equation (4) expresses the specific method of extracting the pseudorange bias. Through the time group delay (TGD) parameter in the broadcast ephemeris, the datum of the pseudorange can be corrected from the L1P to the L1P/L2P combination. Then, through the grid ionospheric correction, theoretically, the mutual difference between the pseudorange of L1P after corrected TGD and the pseudorange of L1P/L2P should only include the residual correction of the ionospheric delay and noise, which should be small and can be considered as white noise with zero mean. However, due to the presence of pseudorange bias, this value can reach the meter level at most.

$$P_{L1CA} - DCB_{p1c1} - tgd_{LNAV} - \frac{TEC}{f_{L1P}} - P_{L1P/L2P} = DCB^{r}_{L1P-L1P/L2P} + \alpha_{L1P-L1P/L2P} \quad (4)$$

where P_{L1CA} is the pseudorange of L1CA; DCB_{p1c1} is the DCB between L1CA and L1P; tgd_{LNAV} is the TGD from the broadcast ephemeris; $\frac{TEC}{f_{L1P}}$ is the ionospheric grid delay;

$P_{L1P/L2P}$ is the pseudorange of the L1P/L2P dual-frequency combination; $DCB^r_{L1P-L1P/L2P}$ is the receiver DCB parameter between L1P and L1P/L2P; $\alpha_{L1P-L1P/L2P}$ is the pseudorange bias between L1P and L1P/L2P.

Through Equation (4), the normal equation can be constructed by multi-station and multi-satellite data. Since the equations are rank-deficient at this time, a priori constraint needs to be introduced. By fixing the DCB of the master monitoring receiver, the equation is solved, and the pseudorange bias of each satellite can be obtained by the least squares.

$\alpha_{L1P-L1P/L2P}$ is the pseudorange bias correction between the L1P and L1P/L2P. The $\alpha_{L1P-L1P/L2P}$ calculated of each satellite is corrected from the satellite clock correction calculated with GPS L1P/L2P to obtain the new satellite clock correction, which is broadcasted to SBAS users, as shown in Equation (5).

$$d_{clk} = d_{oriclk} - \alpha_{L1P-L1P/L2P} \tag{5}$$

where d_{oriclk} is the satellite clock correction calculated with GPS L1P/L2P, and the d_{clk} is the satellite clock correction broadcasted by SBAS RTCA service, which has deducted the pseudorange bias.

2.3. Method to Evaluate the Performance of BDSBAS

For BDSBAS L1C/A single-frequency users, the pseudorange observation equation is shown in Equation (6), the pseudorange is corrected with SBAS long-term correction, fast correction, and ionospheric grid correction to improve the positioning accuracy.

$$P^i_{r1}(L1CA) = \rho^i_{r1} + c * (\delta t_{r1} - \delta t^i) + c * (DCB_{r1} + DCB^i) + T^i_{r1} + rel^i_{r1} + \alpha^i_{r1}(L1P - L1P/L2P) + \varepsilon^i_{r1} + d_{cor} \tag{6}$$

$$d_{cor} = d_{wadp} + d_{clk} + d_{fastclk} + d_{grid} \tag{7}$$

where $P^i_{r1}(L1CA)$ is pseudorange; ρ^i_{r1} is the range between the satellite and receiver; δt_{r1} and δt^i are the clock errors of the receiver and satellite, respectively; T^i_{r1} is the tropospheric delay correction; rel^i_{r1} is the relativity correction; ε^i_{r1} are multipath noises; $\alpha^i_{r1}(L1P - L1P/L2P)$ is the pseudorange bias that needs to be corrected; d_{cor} is the SBAS corrections which are broadcasted by GEO satellites; d_{wadp} is the orbit correction; d_{clk} is the satellite clock correction, which is as same as the satellite clock correction in Equation (5); $d_{fastclk}$ is the fast satellite clock correction; and d_{grid} is the ionospheric grid correction.

For SBAS B1C/B2a dual-frequency users, only long-term correction information is used, and the observation equation is shown in Equation (8).

$$P^i_{r1}(B1C/B2a) = \rho^i_{r1} + c * (\delta t_{r1} - \delta t^i) + c * (DCB_{r1} + DCB^i) + T^i_{r1} + rel^i_{r1} + \varepsilon^i_{r1} + d_{wadp} + d_{clk} \tag{8}$$

The parameters to be estimated were the user's three-dimensional (3-D) position and the receiver clock error in the observation equations, with at least 4 satellites and corresponding SBAS corrections. The estimated position coordinates were compared with the precise known coordinates in BeiDou Coordinate System (BDCS) [35,36], to obtain the positioning errors.

Integrity and availability are important indicators for evaluating the performance of the SBAS service. The integrity parameters are the detection of differential corrections, which assure the reliability of corrections for users. If the accuracy of the different corrections of a certain satellite is high enough, the integrity parameters will be small enough, otherwise it will be large. Similarly, if the satellite is not monitored, the integrity parameters must be broadcasted as unmonitored. If the satellite is abnormal, it must be unavailable. The integrity parameters broadcasted by the SBAS service are used to calculate the Protection Level (PL). It is a predictable value for positioning errors given reasonable assumptions regarding the expected error characteristics, and describes the region assured to contain the indicated position. As the service targets of the BDSBAS are APV-1 and CAT-1, on the basis of guaranteeing integrity, it puts forward higher requirements for its high real-time services. Availability is also achieved through the PL, and the HPL and VPL need to meet

the requirements below the horizontal alert limit (HAL) and vertical alert limit (VAL). For APV-1, HAL = 40 m and VAL = 50 m; for CAT-1, HAL = 40 m and VAL = 10~15 m. The availability is evaluated in seconds. When the condition of PE < PL < AL is satisfied, the latter is considered available. (Figure 2)

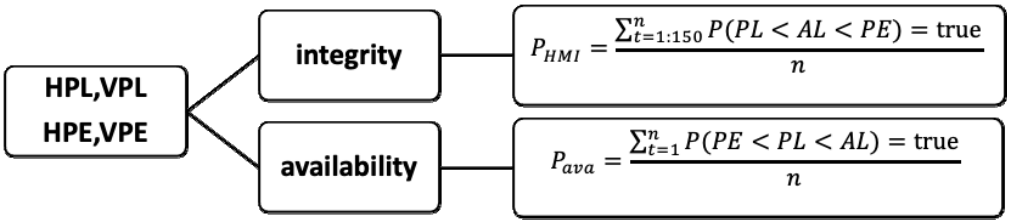

Figure 2. Process to calculate the integrity and availability.

The PL is an important indicator for evaluating the integrity and availability of SBAS. For sat_i, the observation vector is shown in Equation (9).

$$B(i) = \begin{bmatrix} -\cos(ele_i) \times \sin(az_i) & -\cos(ele_i) \times \cos(az_i) & -\sin(ele_i) & 1 \end{bmatrix} \quad (9)$$

where ele_i is the satellite altitudinal angle and az_i is the azimuth. In the same epoch, the observation vectors of different satellites form an observation matrix. The covariance matrix can be calculated by $(\mathrm{B^T PB})^{-1}$, and the elements of the diagonal in the covariance matrix represent the variance in different directions (N, E, U) and the receiver clock error. The weight matrix P is a diagonal matrix composed of the residual error variances of different satellites, $P = diag(\frac{1}{\sigma_i^2}, \ldots, \frac{1}{\sigma_n^2})$. σ_i^2 is shown in Equation (10).

$$\sigma_i^2 = \sigma_{i,fit}^2 + \sigma_{i,UIRE}^2 + \sigma_{i,air}^2 + \sigma_{i,tropo}^2 \quad (10)$$

where $\sigma_{i,fit}^2$ is the model variance for the long-term, fast, and range-rate correction errors; $\sigma_{i,UIRE}^2$ is the model variance for the slant-range ionospheric error; $\sigma_{i,air}^2$ is the model variance for the multipath and noise errors; and $\sigma_{i,tropo}^2$ is the model variance for the tropospheric delay error. After the weight matrix is determined, the covariance matrix can be calculated.

$$d_{major} = \sqrt{\frac{d_{east}^2 + d_{north}^2}{2} + \sqrt{\left(\frac{d_{east}^2 - d_{north}^2}{2}\right)^2 + d_{EN}^2}} \quad (11)$$

In Equation (11), d_{east}^2, d_{north}^2, d_{EN}^2 and d_U^2 are elements of the covariance matrix, which means the variance of errors in different directions. d_{major} is the semi-major axis of the error ellipse. Then, the HPL and VPL are calculated as follows:

$$\begin{aligned} HPL &= K_v \times d_{major} \\ VPL &= K_H \times d_U \end{aligned} \quad (12)$$

In the precision approach mode, K_v = 5.33; K_H = 6.

With respect to the latest DFMC protocol, the calculation of the PL of the dual-frequency receiver is different from RTCA in the construction of the observation matrix and the calculation of the weight matrix. The DFMC is the focus of compatibility and interoperability of various SBAS, so the constellation where the satellite is located is reflected in the observation matrix. The observation vector is shown in Equation (13).

$$B(i) = \begin{bmatrix} -\cos(ele_i) \times \sin(az_i) & -\cos(ele_i) \times \cos(az_i) & -\sin(ele_i) & 1 & n_i \end{bmatrix} \quad (13)$$

If at least two constellations are used and the satellite belongs to the first constellation, n_i = 0; if the satellite is from the second constellation, n_i = 1. For the weight matrix,

the model variance for the slant-range ionospheric error can be ignored because of the dual-frequency combination.

$$\sigma_i^2 = \sigma_{i,DFC}^2 + \sigma_{i,air}^2 + \sigma_{i,tropo}^2 \quad (14)$$

where $\sigma_{i,DFC}^2$ is the model variance for the residual errors.

With the HPL and VPL, as well as HPE and VPE values calculated, the ability of the service integrity and availability can be analyzed.

PL and PE are used as input parameters to compute the integrity and availability. When calculating the probability of HMI, with 150 s of data in one group, the probability of satisfying PL < AL < PE in the group is counted. When calculating the availability, in the continuous monitoring period, with 1s of data in one group, the probability of satisfying PE < PL < AL in the group is counted. If any one of the horizontal or vertical directions does not satisfy the condition, it is considered that the statistical condition is not satisfied.

3. Data and Processing Strategies

By the collocated receiver method, the pseudorange bias we extracted is a relative, not absolute, error. However, this is exactly what we need, which can prove that there is a pseudorange bias between receivers in different statuses. To extract the pseudorange bias based on the collocated receiver method, we need to choose a reference satellite to make double difference. Therefore, in the validity period of the experimental data, we randomly selected a satellite that could be tracked for at least a few hours. In this paper, satellite G29 was selected as the reference satellite, and the pseudorange biases for the GPS L1P and GPS L1P/L2P dual-frequency combinations were calculated with the collocated-receiver observations from 25 August 2020. Then, based on the method described in Section 2.2, we calculated the GPS pseudorange bias between L1P and L1P/L2P by multi-station data from 1 September 2020 to 30 September 2020.

To analyze the service accuracy of the BDSBAS, the positioning errors for GPS L1C/A single-frequency and BDS-3 B1C/B2a dual-frequency were calculated respectively and compared with the results of open services.

(1) Single point positioning (SPP).
(2) SPP with differential SBAS corrections.

The positioning accuracy is expressed with 95% of positioning errors. Five monitoring stations of BDSBAS were selected to evaluate the positioning accuracy, which don't participate in the solving of corrections are selected. The five stations are located in Hebei, Heilongjiang, Zhejiang, Inner Mongolia, and Hainan, China. The SBAS positioning results from 1 September 2020 to 30 September 2020 were calculated. Based on the analysis of SBAS positioning accuracy, the same measuring stations were selected to evaluate the integrity and availability of BDSBAS for a total of 30 days, from 1 September 2020 to 30 September 2020.

4. Results and Analysis

4.1. Results of Pseudorange Bias

Based on the equation and the processing strategies, the time series of pseudorange biases are shown in Figures 3 and 4. Different colors indicate different satellites. The statistical results of pseudorange biases for the GPS L1P single and GPS L1P/L2P dual-frequency combination are shown in Table 1.

In Figures 3 and 4, the results show the pseudorange bias of GPS L1P and L1P/L2P. We can not only see the convergence at the beginning of the arc, but also can find an obvious stratification between double difference of different satellites, and it is the pseudorange bias we need to reduce. As L1P/L2P can amplify the impact of multipath and pseudorange bias, the convergence process and stratification in Figure 4 are more obvious in Figure 3. Table 2 shows the pseudorange bias between GPS L1P and L1P/L2P.

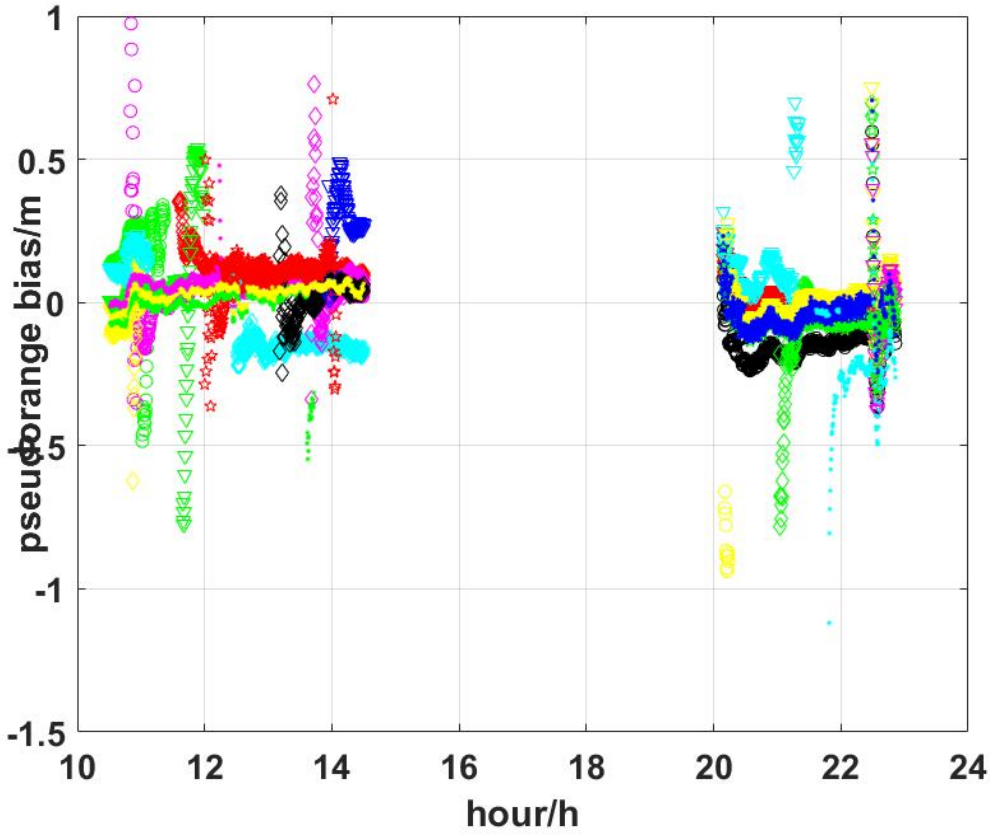

Figure 3. Pseudorange biases in the GPS L1P signal.

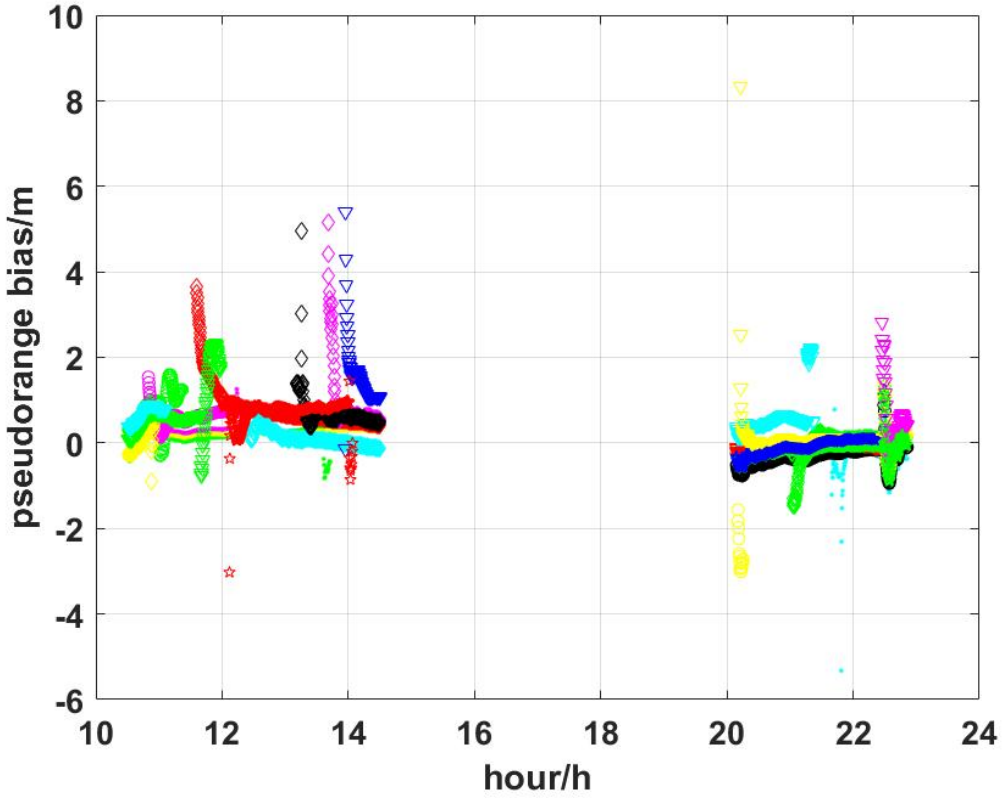

Figure 4. Pseudorange biases in the GPS L1CA/L2P signal.

Table 1. Pseudorange bias of GPS L1P and L1P/L2P.

PRN	Pseudorange Bias/m		PRN	Pseudorange Bias/m	
	L1P	L1P/L2P		L1P	L1P/L2P
G02	0.1	0.2	G19	0.1	0.4
G03	0.1	0.2	G20	0.2	1.3
G04	0.3	0.6	G21	0.1	0.8
G05	0.0	0.2	G22	0.0	0.1
G06	0.1	0.3	G23	0.2	0.9
G09	0.2	0.9	G24	0.3	1.6
G10	0.1	0.4	G25	0.2	0.7
G12	0.3	1.0	G26	0.1	0.4
G13	0.1	0.6	G27	0.2	0.9
G14	0.2	0.4	G30	0.1	0.8
G15	0.1	0.9	G31	0.1	0.3
G16	0.2	0.4	G32	0.1	0.2
G18	0.2	0.2			
MEAN	L1CA:0.14 m		MEAN	L1CA/L2P:0.59 m	
RMS	L1CA:0.17 m		RMS	L1CA/L2P:0.70 m	

Table 2. Pseudorange bias between GPS L1P and L1P/L2P.

PRN	Pseudorange Bias/m			PRN	Pseudorange Bias/m		
	MEAN	RMS	STD		MEAN	RMS	STD
G01	0.57	0.57	0.05	G17	−0.15	0.15	0.03
G02	−1.09	1.09	0.00	G18	−0.09	0.09	0.04
G03	0.80	0.80	0.06	G19	−1.57	1.57	0.02
G04	−0.09	0.09	0.02	G20	−0.92	0.92	0.01
G05	0.27	0.27	0.04	G21	−1.01	1.02	0.04
G06	0.90	0.90	0.02	G22	−1.25	1.25	0.05
G07	0.30	0.30	0.02	G23	−0.27	0.27	0.01
G08	0.46	0.46	0.03	G24	0.63	0.63	0.03
G09	0.15	0.16	0.04	G25	0.02	0.06	0.06
G10	0.25	0.25	0.01	G26	0.16	0.16	0.02
G11	−0.50	0.50	0.05	G27	0.40	0.40	0.02
G12	−0.13	0.13	0.02	G28	−0.57	0.57	0.01
G13	−0.04	0.05	0.03	G29	−0.25	0.25	0.05
G14	0.01	0.01	0.00	G30	0.01	0.03	0.02
G15	0.20	0.20	0.06	G31	0.49	0.49	0.05
G16	−0.35	0.35	0.01	G32	0.59	0.59	0.04

The results show that the pseudorange biases for the L1P/L2P dual-frequency combination are obviously larger than those for the L1P signal, as amplified by the dual-frequency combination factor. The average pseudorange bias is approximately 0.59 m on the L1P/L2P dual-frequency combination and approximately 0.14 m on the L1P signal for the adopted collocated receivers. For the RMS, it is approximately 0.70 m on the L1P/L2P dual-frequency combination and approximately 0.17m on the L1P signal.

Statistics show that the influence of pseudorange bias reaches the decimeter level or even the meter level, and the stratification between different satellites is very obvious, and it can also reach the decimeter level or even the meter level. The differential corrections of SBAS are usually computed with dual-frequency ionospheric-free combinations. If the pseudorange bias errors of monitoring receivers are not well considered and addressed, the differential corrections of SBAS will include the pseudorange bias errors, and the service accuracy of SBAS will be seriously affected.

Based on the Equation (4) and the processing strategies in Section 3, the GPS pseudorange biases between L1P and L1P/L2P are shown in Figure 5 and Table 2.

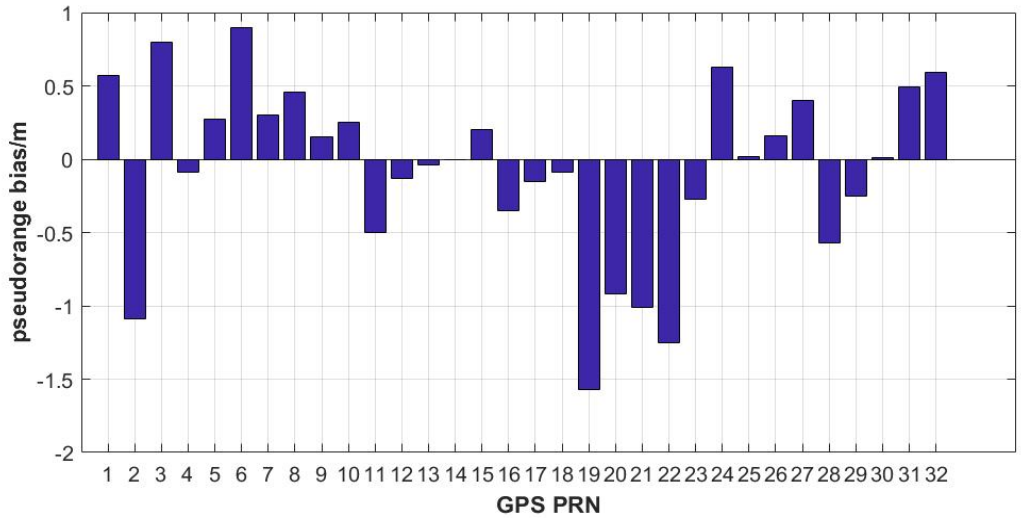

Figure 5. Pseudorange bias correction of GPS satellites.

Figure 5 shows that most of the satellites' pseudorange biases can reach the magnitude of decimeter and can be up to 1.57 m, such as G19. This means that the magnitude of the pseudorange bias can have a great impact on the service performance of the BDSBAS RTCA service. Therefore, if it is corrected in the long-term satellite clock correction and broadcast to the user, the influence of the pseudorange bias on the accuracy of the differential corrections can be reduced. Table 2 shows the statistical results of pseudorange bias for 30 days. The results show that the pseudorange bias has good stability, within about 6 cm.

In addition, Figure 6 shows that the pseudorange biases of GPS BlockIII (G04, G18 and G23) are the smallest, with a maximum of 0.27 m. Additionally, the satellites for which pseudorange biases are longer than 1m are all GPS BlockIIR (G02, G19, G21 and G22). The preliminary results show that with the update of GPS satellites, the nonideal characteristics of downlink navigation signals are gradually improving, and the pseudorange bias is also suppressed.

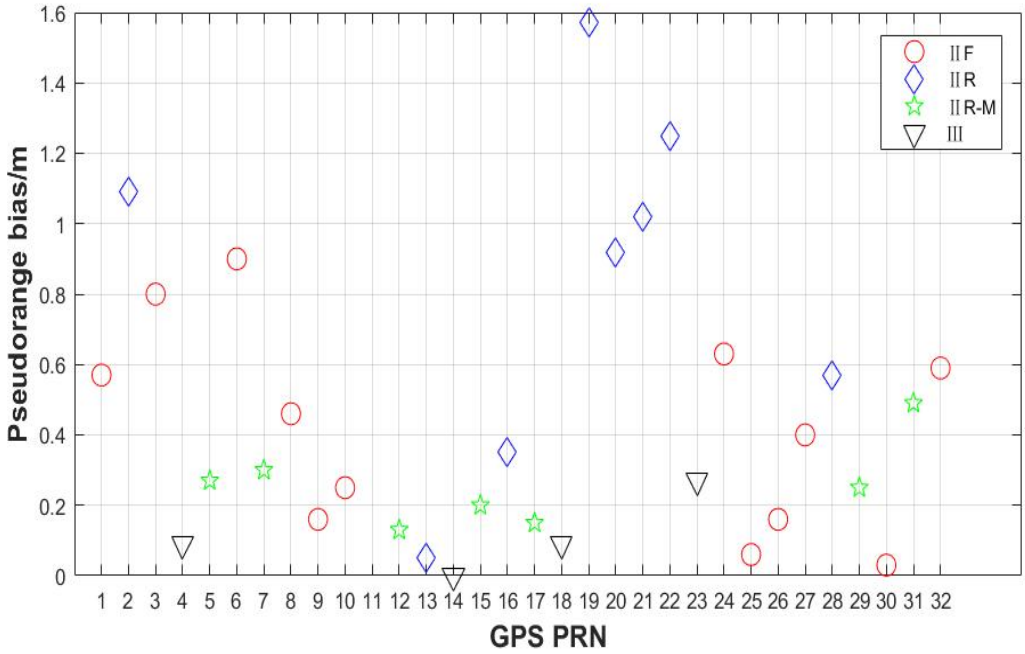

Figure 6. Pseudorange bias of different GPS satellites.

Based on the results of Figure 5, we follow the Equation (5) and Figure 1, and acquire the new satellite clock correction by deducting the pseudorange bias. With two kinds of satellite clock corrections, one kind is modified with pseudorange biases while the other is not, and the differential positioning accuracies for a monitoring receiver are compared, as shown in Figure 7. In the top subgraph, the satellite clock corrections adopted are not corrected with the pseudorange bias, and in the bottom subgraph, the satellite clock corrections are corrected with the pseudorange bias.

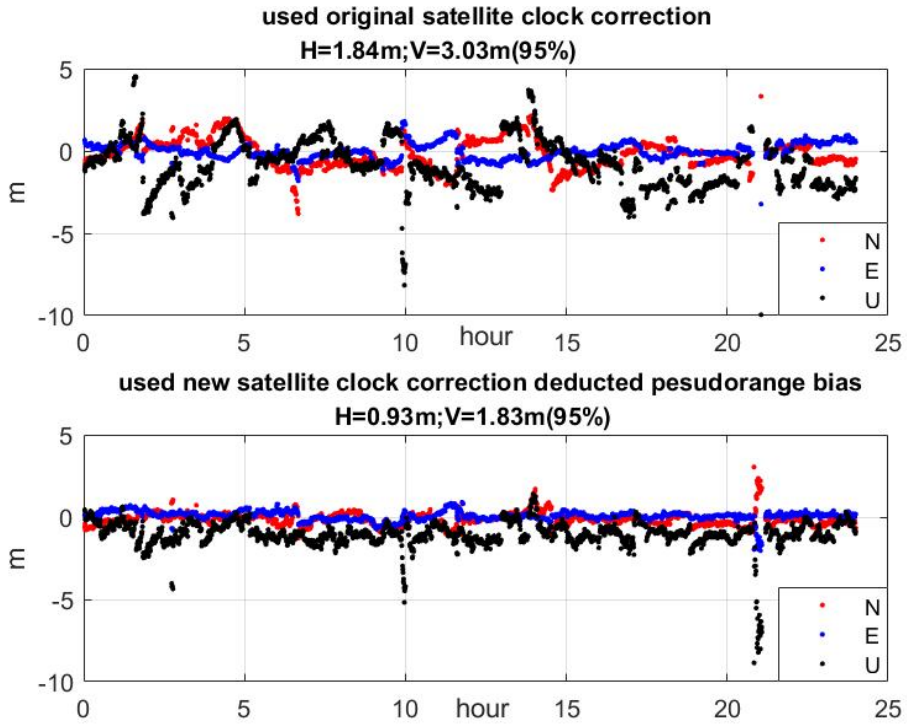

Figure 7. SPP results if deducted pseudorange bias.

It shows that if the satellite clock correction is corrected with the pseudorange bias, the positioning accuracy of SBAS could be improved by about 50% and 40% in horizontal and vertical directions, respectively. The pseudorange bias is an important source of error which could seriously affect the service performance of the SBAS RTCA service.

4.2. Performance of BDSBAS

It can be seen from Tables 3 and 4 that, compared to open service, the positioning accuracy is significantly improved by applying the differential corrections. For GPS L1C/A single-frequency users, the positioning accuracy could be improved by about 47% in 3-D direction, and for BDS-3 B1C/B2a dual-frequency users, approximately 36% improvement is achieved. With the BDSBAS differential corrections, the positioning accuracy can be effectively improved for both single-frequency and dual-frequency users.

Table 3. L1C/A single-frequency positioning accuracy statistics (95% error).

	GPS Open Service			**SBAS**		
Station	Horizontal/m	Vertical/m	3-D/m	Horizontal/m	Vertical/m	3-D/m
Station 01	1.76	4.29	4.41	0.81	2.13	2.20
Station 02	1.81	3.98	4.08	0.94	1.76	1.90
Station 03	2.11	3.74	3.97	1.18	2.90	3.02
Station 04	1.94	3.94	4.12	0.96	2.39	2.46
Station 05	1.66	4.10	4.22	0.84	1.33	1.43
mean	1.86	4.01	4.16	0.95	2.10	2.20

Table 4. B1C/B2a dual-frequency positioning accuracy statistics (95% error).

	BDS-3 Open Service			SBAS		
Station	Horizontal/m	Vertical/m	3-D/m	Horizontal/m	Vertical/m	3-D/m
Station 01	0.88	1.21	1.38	0.34	0.66	0.74
Station 02	0.87	1.28	1.46	0.51	0.88	0.99
Station 03	0.92	1.73	1.85	0.57	1.12	1.20
Station 04	0.90	1.55	1.67	0.58	1.02	1.11
Station 05	1.09	1.75	1.99	0.67	1.18	1.33
mean	0.93	1.50	1.67	0.53	0.97	1.07

The performance of regional availability represents the reliability and correctness of the differential corrections and integrity information of the BDSBAS in the service area. Based on the enhanced products broadcast by the BDSBAS, the PL is calculated, and the availability of BDSBAS RTCA and DFMC services within the service area are analyzed and evaluated, with a spatial resolution of 5° × 5° and a frequency of 1 Hz (Figures 8 and 9). The statistical method refers to the method in Figure 2. If the condition of PE < PL < AL is satisfied, the grid point is considered available. The total sampling time is 30 days, and the final result of each grid point is the average of 30 days.

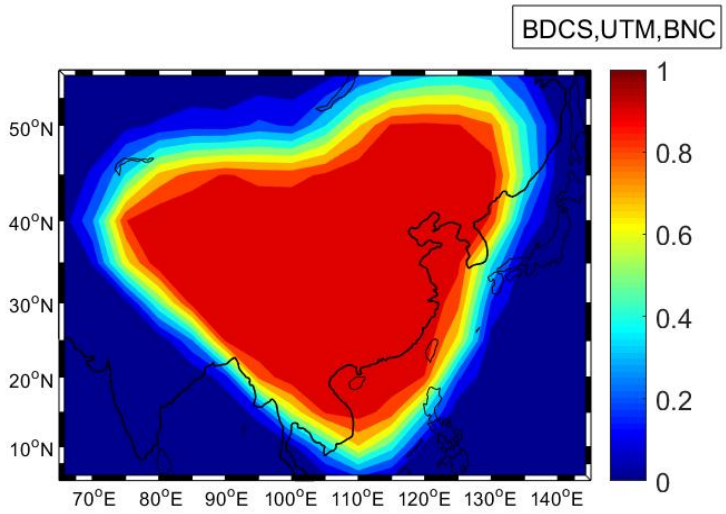

Figure 8. Regional availability of the BDSBAS RTCA service.

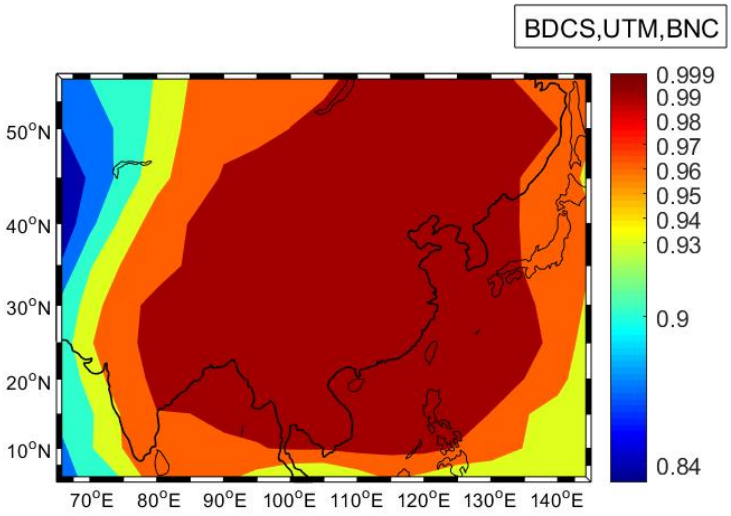

Figure 9. Regional availability of the BDSBAS DFMC service.

It can be seen from Figures 8 and 9 that the availability of RTCA services in central and southern China is the best, but the availability is significantly lower in border areas such as the northeast (125°E, 50°N), the border of Inner Mongolia (110°E, 45°N), and northern Xinjiang (80°E, 45°N). Compared to DFMC services, the availability in China can reach 99.9%, and there is better availability in the surrounding areas.

Based on the results of regional availability, combined with the PEs of each station calculated in Section 2.3, the statistics of the availability of each station and the integrity of each station are analyzed. Table 5 shows the 30-day availability statistics of each station.

Table 5. BDSBAS availability statistics.

Station	RTCA Service		DFMC Service	
	Availability	**Integrity**	**Availability**	**Integrity**
Station 01	100%	0	100%	0
Station 02	99.95%	0	100%	0
Station 03	97.58%	0	100%	0
Station 04	96.82%	0	100%	0
Station 05	100%	0	100%	0
mean	98.87%	0	100%	0

It can be seen that, in the detection period, the integrity risk probability is 0, and there is no HMI. Table 4 shows that for the DFMC services, the availability of the 5 stations can reach 100%. This result is consistent with Figure 8. For RTCA services, the availability of stations in the central and southern regions can reach 100%, such as Station 1 and Station 5. However, some of the border areas in the northeast and west have relatively poor availability, such as Station 3 and Station 4.

Since the availability and integrity are evaluated through the PL, to a large extent, the availability result represents the envelope capability of integrity. Taking Station 1 as an example, the left is single-frequency and the right is dual-frequency. The results of one day are shown in Figure 10.

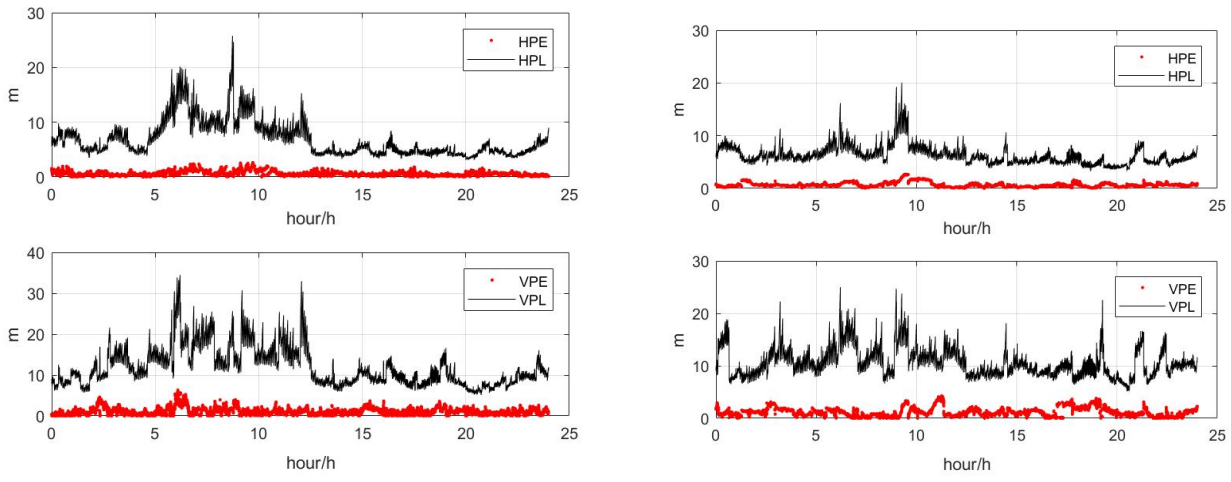

Figure 10. BDSBAS RTCA service and DFMC service integrity of Station 1.

It can be seen from Figure 10 that the PL can completely envelop the PE, which is consistent with the availability result. There are two main reasons for this poor availability: the PL fails to cover the PE, and the PL exceeds the AL. Therefore, if the former leads to poor availability, its envelope integrity will also be poor. If it is the latter, although the availability is poor, the integrity of the envelope capability can reach the standard. Figure 11 is the integrity envelope diagram under the RTCA service of Station 4, which shows the reasons for its poor availability.

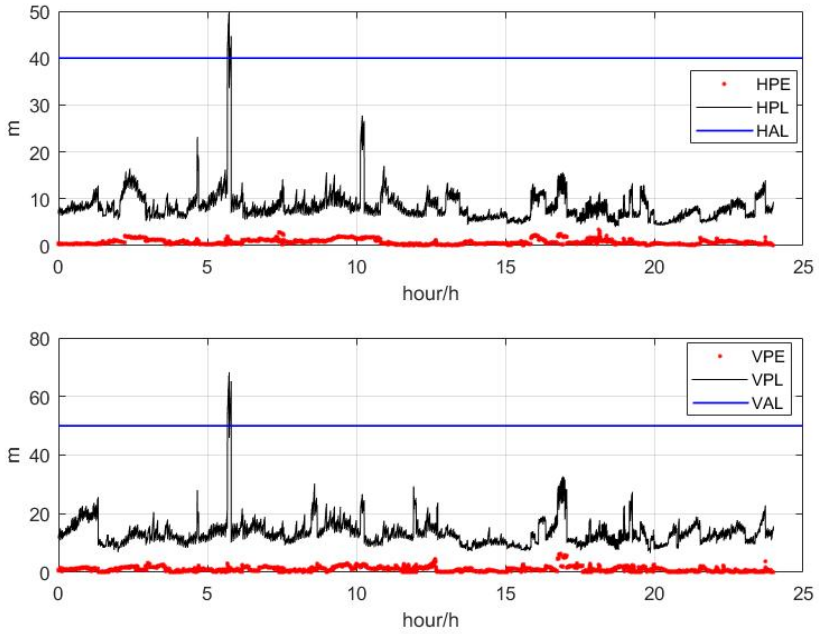

Figure 11. BDSBAS RTCA service integrity of Station 4.

It can be seen from Figure 11 that the envelope of integrity to the PE can reach 100%, but due to the phenomenon that the PL exceeds the AL, its usability is poor, and the availability can't reach 100%. Since RTCA services are limited by the availability of the ionospheric grid, if there are no available grid points for a certain satellite, the satellite will not be used for positioning, which affects the PDOP. Therefore, Figure 12 shows the number of satellites available at Station 4, and Figure 13 shows the availability of IGPs.

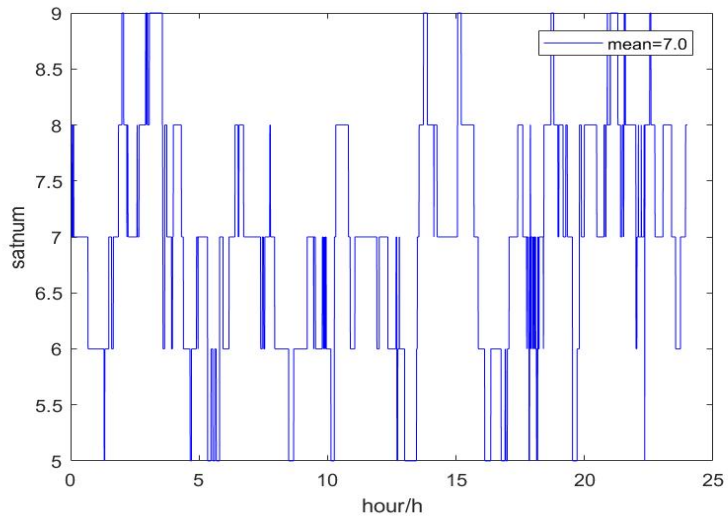

Figure 12. Number of satellites available at Station 4.

The positions of the five stations are marked with purple circles in Figure 13. By combining Figures 12 and 13, we find that when the number of available satellites decreases, the HPL and VPL will gradually increase. In the period when the PL exceeds the limit in Figure 11, only five satellites are available. When the number of satellites increases to six or more, the PL will gradually decrease. Through further analysis, because Station 4 is located in Inner Mongolia, which is the border area of China, the puncture point of the visible satellite of Station 4 falls outside the service area during this period. There are few grid points in this area, which does not satisfy the fitting conditions and makes the satellite not available during positioning; this phenomenon leads to an increase in the PDOP value.

Compared with the PE, the PL is more sensitive to changes in the PDOP value, resulting in a significant increase in the PL. Therefore, under the premise that the differential correction information and integrity information are normal, the availability of IGPs is one of the important factors that affect the availability.

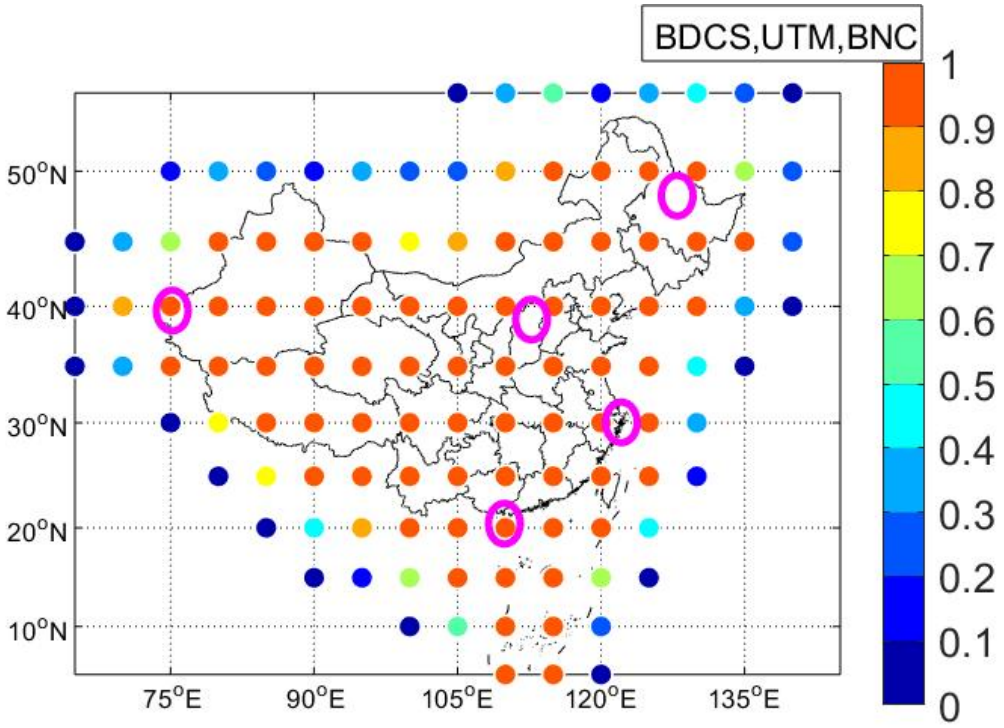

Figure 13. Availability of IGPs.

5. Conclusions and Discussion

This article mainly analyzes the pseudorange bias that affects the performance of BDSBAS services and provides the magnitude of the effect of the pseudorange bias on the performance of SBAS services. Through experiments, we conclude that the pseudorange bias will have a greater effect on the performance of single-frequency SBAS services. The results show that the GPS pseudorange biases between L1P and L1P/L2P can be up to 1.57 m and have good stability over 30 days, within about 6 cm. In addition, by collecting observation data from 1 September 2020 to 30 September 2020, the accuracy and availability of single-frequency and dual-frequency SBAS positioning were studied and analyzed, and the following conclusions were drawn:

(1) The differential correction information broadcast by the BDSBAS can effectively improve the positioning accuracy of the users. For single-frequency users, since the effect of the pseudorange bias is absorbed in the long-term satellite clock corrections, the differential corrections significantly affect single-frequency users. When the pseudorange bias was solved and corrected in satellite clock corrections, the performance of BDSBS can be improved.

(2) The availability of RTCA services can reach 99.9% in central China, and the availability of ionospheric grid points is one of the important factors that affect its service performance; the availability of DFMC services in China can reach 99.9%; in some surrounding areas, and they can also have no less than 99% availability.

(3) The results show that the pseudorange biases of GPS BlockIII are the smallest, and the satellites which have the largest pseudorange bias are all GPS BlockIIR. This shows that with the update of GPS satellites, the nonideal characteristics of downlink navigation signals are gradually improving, and the pseudorange bias is also suppressed. We need to pay more attention to this aspect in the follow-up work.

Based on the current test results, the BDSBAS can basically provide dual-frequency enhanced services, but the DFMC protocol has not been finalized and there is no clear direction for the compatibility and interoperability of different SBAS systems. Therefore, the next step is to study the performance of SBAS services of multiple systems in the same service area.

The availability of the grid points is currently one of the main factors that affects the positioning accuracy and availability of SBAS RTCA services. Limited by the distribution of measurement stations, the resolution and availability rate of the grid in the border area are low, and the grid cannot contain all satellite piercing points. Therefore, improving the grid availability in border areas is one of the focuses of future work. In addition, there is no clear division of the service area of BDSBAS, but integrity and availability are important considerations in determining the service area. Further improving the availability of services and the division of service areas is also one of the next steps.

Author Contributions: Conceptualization, Y.C., C.T., S.Z. and X.H.; methodology, Y.L., L.Z. and J.C.; software, Y.L. and Q.T.; Validation, Y.L.; Formal analysis, Y.L. and Q.T; investigation, Y.L.; resources, J.C. and Y.Y; data curation, Y.L. and Y.Y.; writing—original draft preparation, Y.L.; writing—review and editing, Y.L.; visualization, Y.L.; supervision, Y.C.; project administration, Y.C.; funding acquisition, Y.C. and S.Z. All authors have read and agreed to the published version of the manuscript.

Funding: This study is supported by the National Natural Science Foundation of China (Grant No. 41574029, 41674041, 41874039 and 12173072).

Data Availability Statement: Not applicable.

Acknowledgments: This study is supported by the National Natural Science Foundation of China. And thanks for the help of Shanghai Astronomical Observatory, University of Chinese Academy of Sciences, Beijing Navigation Center and Space Star Technology CO., LTD.

Conflicts of Interest: The authors declare no conflict of interest.

References

1. Zhang, X.; Wu, M.; Liu, W.; Li, X.; Yu, S.; Lu, C.; Wickert, J. Initial assessment of the COMPASS/BeiDou-3: New-generation navigation signals. *J. Geod.* **2017**, *91*, 1225–1240. [CrossRef]
2. Zhou, S.; Hu, X.; Wu, B.; Liu, L.; Qu, W.; Guo, R.; He, F.; Cao, Y.; Wu, X.; Zhu, L.; et al. Orbit determination and time synchronization for a GEO/IGSO satellite navigation constellation with regional tracking network. *Sci. China Ser. G Phys. Mech. Astron.* **2011**, *54*, 1089–1097. [CrossRef]
3. Zhou, S.; Cao, Y.; Zhou, J.; Hu, X.; Tang, C.; Liu, L.; Guo, R.; He, F.; Chen, J.; Wu, B. Positioning accuracy assessment for the 4GEO/5IGSO/2MEO constellation of COMPASS. *Sci. China Ser. G Phys. Mech. Astron.* **2012**, *55*, 2290–2299. [CrossRef]
4. ICAO. *International Standards and Recommended Practices (SARPS), Annex 10—Aeronautical Telecommunications*; Radio Navigation Aids 2006; ICAO: Montreal, QC, Canada, 2006.
5. SBAS IWG. *SBAS L5 DFMC Interface Control Document (SBAS L5 DFMC ICD)*; Revision 4; SBAS IWG: Dakar, Senegal, 2017.
6. RTCA. *Minimum Operational Performance Standards for Global Positioning System/Wide Area Augmentation System Airborne Equipment, RTCA DO-229D*; RTCA, Inc.: Washington, DC, USA, 2006.
7. RTCA. *Minimum Operational Performance Standards for Global Positioning System/Wide Area Augmentation System Airborne Equipment: Integrated and Highlighted*; RTCA, Inc.: Washington, DC, USA, 2013.
8. Cao, Y.; Hu, X.; Wu, B.; Zhou, S.; Liu, L.; Su, R.; Chang, Z.; He, F.; Zhou, J. The wide-area difference system for the regional satellite navigation system of COMPASS. *Sci. China Ser. G Phys. Mech. Astron.* **2012**, *55*, 1307–1315. [CrossRef]
9. Cabler, H.; De Cleene, B. LPV: New, Improved WAAS Instrument Approach. In Proceedings of the International Technical Meeting of the Satellite Division of the Institute of Navigation, Portland, OR, USA, 24–27 September 2002.
10. Chen, J.; Huang, Z.G.; Li, R. Computation of satellite clock–ephemeris corrections using a priori knowledge for satellite-based augmentation system. *GPS Solut.* **2017**, *21*, 663–673. [CrossRef]
11. Zhao, L.; Hu, X.; Tang, C.; Cao, Y.; Zhou, S.; Yang, Y.; Liu, L.; Guo, R. Generation of DFMC SBAS corrections for BDS-3 satellites and improved positioning performances. *Adv. Space Res.* **2020**, *66*, 702–714. [CrossRef]
12. Xu, A.; Xu, Z.; Ge, M.; Xu, X.; Zhu, H.; Sui, X. Estimating Zenith Tropospheric Delays from BeiDou Navigation Satellite System Observations. *Sensors* **2013**, *13*, 4514–4526. [CrossRef] [PubMed]
13. Zhang, X.; Guo, F.; Zhou, P. Improved precise point positioning in the presence of ionospheric scintillation. *GPS Solut.* **2014**, *18*, 51–60. [CrossRef]
14. Shallberg, K.; Shloss, P.; Altshuler, E.; Tahmazyan, L. *WAAS Measurement Processing, Reducing the Effects of Multipath*; ION GPS 2001; ION: Salt Lake City, VA, USA, 2001; pp. 2334–2340.

15. Wu, X.; Zhou, J.; Wang, G.; Hu, X.; Cao, Y. Multipath error detection and correction for GEO/IGSO satellites. *Sci. China Ser. G Phys. Mech. Astron.* **2012**, *55*, 1297–1306. [CrossRef]
16. Wong, G.; Phelts, R.E.; Walter, T.; Enge, P. Bounding errors caused by nominal gnss signal deformations. In Proceedings of the 24th International Technical Meeting of the Satellite Division of the Institute of Navigation (ION GNSS 2011), Portland, OR, USA, 20–23 September 2011; Volume 6955, pp. 2657–2664.
17. Wong, G.; Phelts, R.E.; Walter, T.; Enge, P. Characterization of signal deformations for gps and waas satellites. In Proceedings of the 23rd International Technical Meeting of the Satellite Division of the Institute of Navigation (ION GNSS 2010), Portland, OR, USA, 21–24 September 2010; Volume 7672, pp. 3143–3151.
18. Gong, X.; Lou, Y.; Zheng, F.; Gu, S.; Shi, C.; Liu, J.; Jing, G. Evaluation and calibration of BeiDou receiver-related pseudorange biases. *GPS Solut.* **2018**, *22*, 98. [CrossRef]
19. Phelts, R.E.; Akos, D.M.; Enge, P. Robust signal quality monitoring and detection of evil waveforms. In Proceedings of the ION NTM 2000, Institute of Navigation, Anaheim, CA, USA, 26–28 January 2000; pp. 1180–1190.
20. Grewal, M.S. Space-based augmentation for global navigation satellite systems. *IEEE Trans. Ultrason. Ferroelectr. Freq. Control.* **2012**, *59*, 497–503. [CrossRef] [PubMed]
21. Cao, Y.L.; Hu, X.G.; Zhou, J.H.; Wu, B. Kinematic Wide Area Differential Corrections for BeiDou Regional System basing on two-way Time Synchronization. *Lect. Notes Electr. Eng.* **2014**, *305*, 277–288.
22. Wong, G.; Chen, Y.H.; Phelts, R.E.; Walter, T.; Enge, P. Mitigation of Nominal Signal Deformations on Dual-Frequency WAAS Position Errors. In Proceedings of the 27th International Technical Meeting of the Satellite Division of the Institute of Navigation (ION GNSS+ 2014), Tampa, FL, USA, 8–12 September 2014; pp. 3129–3147.
23. Hauschild, A.; Montenbruck, O. A study on the dependency of gnss pseudorange biases on correlator spacing. *GPS Solut.* **2016**, *20*, 159–171. [CrossRef]
24. Hauschild, A.; Montenbruck, O. The Effect of Correlator and Front-End Design on GNSS Pseudorange Biases for Geodetic Receivers. *Navigation* **2016**, *63*, 443–453. [CrossRef]
25. Tang, C.; Guo, R.; Hu, X.; Zhu, L.; Li, R.; Pan, J.; Zhou, S.; Chen, J. Orbit determination and time synchronization for new-generation Beidou satellites: Preliminary results. *Sci. Sin. Phys. Mech. Astron.* **2016**, *46*, 119502. [CrossRef]
26. Felski, A.; Nowak, A. On Egnos Monitoring in Local Conditions. *Artif. Satell.* **2013**, *48*, 85–92. [CrossRef]
27. Felski, A.; Nowak, A.; Woźniak, T. Accuracy and Availability of Egnos—Results of Observations. *Artif. Satell.* **2011**, *46*, 111–118. [CrossRef]
28. Fellner, A.; Banaszek, K.; Trómi´nski, P. The implementation of the EGNOS system to APV-I precision approach operations. *Trans. Nav. Int. J. Mar. Navig. Safe. Sea Transp.* **2010**, *4*, 41–46.
29. Larence, D.; Bunce, D.; Mathur, N.G.; Sigler, C.E. *Wide Area Augmentation System (WAAS)—Program Status*; ION GNSS 2007; ION: Fort Worth, VA, USA, 2007; pp. 892–899.
30. Garcia, A.M.; Medel, C.H.; Merino, M.M.R. *Galileo Navigation and Integrity Algorithms*; ION GNSS 2005; ION: Long Beach, CA, SA, 2005; pp. 1315–1326.
31. Hernandez, C.; Catalan, C.; Fernandez, M.A.; Gavin, A.J.; Sardon, E.; Martin, J.R. *Galileo Integrity: The Ground Segment Comput Algorithm Perspective*; ION GNSS 2006; ION: Fort Worth, TX, USA, 2006; pp. 2634–2645.
32. Amarillo, F.; D'Angelo, P. *New Developments for the User Integrity Processing with Galileo Implementation and Testing of Galileo User Integrity Algorithms*; ION GNSS 2009; ION: Savannah, GA, USA, 2009; pp. 2775–2782.
33. Kovach, K.; Dobyne, J.; Crews, M.; Miles, C. *GPS III Integrity Concept*; ION GNSS 2008; ION: Savannah, GA, USA, 2008; pp. 2250–2257.
34. Steigenberger, P.; Hauschild, A.; Montenbruck, O.; Hugentobler, U. *Performance Analysis of COMPASS Orbit and Clock Determination and COMPASS-Only PPP*; IGS Workshop: Olsztyn, Poland, 2012.
35. Wei, Z.; Liu, G.; Wu, F. Compass Coordinate System. EGU General Assembly Conference. In *Proceedings of the EGU General Assembly Conference Abstracts*; 2013; Available online: https://ui.adsabs.harvard.edu/abs/2013EGUGA..15.6788W (accessed on 15 August 2021).
36. Liu, Y.C.; Liu, L.; Zhou, S.S.; Xu, J.Y.; Qi, W.; Hu, X.G. Research on Accuracy Evaluation Method of Beidou Coordinate Frame. *Prog. Astron.* **2021**, *39*, 105–107. [CrossRef]